Original Article

Diffusion-weighted EPI- and HASTE-MRI and 18F-FDG-PET-CT early during chemoradiotherapy in advanced head and neck cancer

Charlotte S. Schouten[1], Remco de Bree[1], Lisa van der Putten[1], Daniel P. Noij[2], Otto S. Hoekstra[2], Emile F.I. Comans[2], Birgit I. Witte[3], Patricia A. Doornaert[4], C. René Leemans[1], Jonas A. Castelijns[2]

[1]Department of Otolaryngology-Head and Neck Surgery, [2]Department of Radiology and Nuclear Medicine, [3]Department of Epidemiology and Biostatistics, [4]Department of Radiation Oncology, VU University Medical Center, Amsterdam, the Netherlands

Correspondence to: Prof. Dr. Jonas A. Castelijns. Department of Radiology and Nuclear Medicine, VU University Medical Center, De Boelelaan 1117, 1081 HV Amsterdam, The Netherlands. Email: j.castelijns@vumc.nl.

Main problem: Diffusion-weighted MRI (DW-MRI) has potential to predict chemoradiotherapy (CRT) response in head and neck squamous cell carcinoma (HNSCC) and is generally performed using echo-planar imaging (EPI). However, EPI-DWI is susceptible to geometric distortions. Half-fourier acquisition single-shot turbo spin-echo (HASTE)-DWI may be an alternative. This prospective pilot study evaluates the potential predictive value of EPI- and HASTE-DWI and 18F-fluorodeoxyglucose PET-CT (18F-FDG-PET-CT) early during CRT for locoregional outcome in HNSCC.

Methods: Eight patients with advanced HNSCC (7 primary tumors and 25 nodal metastases) scheduled for CRT, underwent DW-MRI (using both EPI- and HASTE-DWI) and 18F-FDG-PET(-CT) pretreatment, early during treatment and three months after treatment. Median follow-up time was 38 months.

Results: No local recurrences were detected during follow-up. Median Apparent Diffusion Coefficient $(ADC)_{EPI}$-values in primary tumors increased from 77×10^{-5} mm^2/s pretreatment, to 113×10^{-5} mm^2/s during treatment (P=0.02), whereas ADC_{HASTE} did not increase (74 and 74 mm^2/s, respectively). Two regional recurrences were diagnosed. During treatment, ADC_{EPI} tended to be higher for patients with regional control $[(117.3\pm12.1)\times10^{-5}$ $mm^2/s]$ than for patients with a recurrence $[(98.0\pm4.2)\times10^{-5}$ $mm^2/s]$. This difference was not seen with ADC_{HASTE}. No correlations between ΔADC_{EPI} and ΔSUV (Standardized Uptake Value) were found in the primary tumor or nodal metastases.

Conclusions: HASTE-DWI seems to be inadequate in early CRT response prediction, compared to EPI-DWI which has potential to predict locoregional outcome. EPI-DWI and 18F-FDG-PET-CT potentially provide independent information in the early response to treatment, since no correlations were found between ΔADC_{EPI} and ΔSUV.

Keywords: Chemoradiotherapy (CRT); diffusion-weighted magnetic resonance imaging (DW-MRI); head and neck squamous cell carcinoma (HNSCC); positron emission tomography (PET); treatment response

Submitted May 23, 2014. Accepted for publication Jul 25, 2014.
doi: 10.3978/j.issn.2223-4292.2014.07.15
View this article at: http://dx.doi.org/10.3978/j.issn.2223-4292.2014.07.15

Introduction

Patients with resectable advanced staged head and neck squamous cell carcinomas (HNSCC) are currently often treated with non-surgical protocols to preserve organ function and to maintain quality of life (1,2). Although chemoradiotherapy (CRT) results in acceptable locoregional control rates, recurrence rates remain considerable (2,3). If residual or recurrent disease is detected after CRT, surgical 'salvage' treatment may be an option, but 'salvage' surgery is often associated with substantial morbidity and complications (4,5). Prediction of treatment outcome early during treatment might avoid ineffective treatment in certain patients and would allow a treatment switch to surgery in these patients (6).

Diffusion-weighted magnetic resonance imaging (DW-MRI) has been suggested as a predictive factor for response of tumor to CRT (7). DW-MRI characterizes tissue based on differences in water mobility, which is related to cellularity (8). These differences can be quantified with Apparent Diffusion Coefficient (ADC): hypercellular tissue (e.g., malignancy) is characterized by a low ADC, whereas hypocellular tissue with necrosis or apoptosis is characterized by a high ADC (9). Conceptually, response to treatment should correspond to an increase in ADC, because treatment-induced loss of tumor cells increases water mobility at the microscopic level. In contrast, residual tumor cells might be detected as decreased ADC-values (10). Several studies have indicated the potential of DW-MRI as a predictor of treatment response in HNSCC (11-13).

DW-MRI in HNSCC is most commonly performed with an echo-planar imaging (EPI)-sequence (11-13). It may be difficult to perform DWI of the head and neck area, because this region is very inhomogeneous and susceptible to artefacts. EPI-DWI is particularly prone to geometric distortions due to susceptibility artefacts (14). DW-MRI is a potential technique for tumor definition in radiotherapy planning, but accurate target definition is essential. Also, with PET/MRI spreading in the clinical field, geometrical accuracy is crucial for fusing PET-images with DW-MRI images. If artefacts with EPI-DWI are too detrimental, a non-EPI method such as half-fourier acquisition single-shot turbo spin-echo (HASTE), may be a better alternative (15). Verhappen *et al*. compared EPI- with HASTE-DWI in HNSCC and concluded that EPI images showed more geometric distortions (15). A comparative study between EPI- and HASTE-DWI in HNSCC for prediction of locoregional control after CRT has not been performed previously.

Tumor metabolism is another potential predictor and can be studied with positron emission tomography (PET). 18F-fluorodeoxyglucose (18F-FDG), a radiolabeled glucose analogue, is used to measure glucose metabolism in malignant tissues. Clinical studies report associations between decline in 18F-FDG uptake in the early phase of CRT and a positive therapy outcome (16-18).

The aim of this pilot study was twofold. First, the purpose was to compare HASTE-DWI with EPI-DWI and 18F-FDG-PET (-CT) early during CRT for their potential to predict locoregional outcome in patients with HNSCC. Secondly, we wanted to correlate changes in ADC- and SUV-values between pretreatment and early during treatment.

Materials and methods

Patients and study design

Eight patients with histological proven advanced (T2, T3 or T4) oro- or hypopharyngeal carcinoma (with a total of 7 primary tumors and 25 lymph node metastases) scheduled for primary CRT with curative intent, were enrolled in this prospective pilot study (*Table 1*). The study was approved by the institutional ethics committee and complies with the Declaration of Helskini. Informed consent was obtained in all patients. Routine pretreatment examinations included 18F-FDG-PET(-CT) (PET_1), MRI and a panendoscopy with biopsies. For study-purposes, EPI- and HASTE-DWI were added ($DW\text{-}MRI_1$). A second MRI with additional DW-MRI ($DW\text{-}MRI_2$) and a second 18F-FDG-PET(-CT) (PET_2) were performed 14 days (±1 day) after the start of radiotherapy (20±2 Gy). $DW\text{-}MRI_2$ and PET_2 were not used for clinical assessment. All patients received cisplatin-based CRT (n=6) or cetuximab-based CRT (n=2). A radiation dose of 70 Gray (Gy) in 2 Gy/fraction was delivered and elective nodal regions received a dose of 54.25-57.75 Gy in 1.55-1.65 Gy/fraction. All patients completed radiotherapy, but toxicity precluded complete cisplatin-CRT in one patient.

During follow-up, patients were regularly examined according to our standard head-and-neck oncology protocol. Routine response evaluation was performed three months after CRT, using DW-MRI ($DW\text{-}MRI_3$), 18F-FDG-PET(-CT) (PET_3) and an examination under general anaesthesia. Median follow-up was 38 months (range, 17-60 months). Additional investigations during follow-up were performed at the discretion of the attending physician. Locoregional control was defined as persistent complete regression of the primary tumor and lymph nodes during follow-up. A timeline illustrating the consecutive

Table 1 Patient and tumor characteristics

No. of patient	Gender	Age	Primary site	T	N	Treatment method	Locoregional recurrence	Salvage surgery	Follow-up
1	M	51	Palatine tonsil	3	2c	Cisplatin-based CRT	LNM[a]	Yes	37 months DM, DOD
2	M	68	Palatine tonsil	2	2b	Cisplatin-based CRT	No	No	60 months NED
3	M	63	Base of tongue	4	2c	Cisplatin-based CRT	No	No	46 months NED
4	M	56	Palatine tonsil	4	3	Cisplatin-based CRT	No	No	39 months NED
5	F	55	Palatine tonsil	2	2a	Cisplatin-based CRT[b]	No	No	37 months NED
6	M	63	Vallecula	3	2c	Cetuximab-based CRT	LNM	No	17 months DM, DOD
7	F	63	Palatine tonsil	2	2b	Cisplatin-based CRT	No	No	35 months NED
8	M	68	Piriform sinus	3	1	Cetuximab-based CRT	No	No	30 months NED

[a], histopathologically proven; [b], toxicity precluded complete chemotherapy; M, male; F, female; age at diagnosis (in years); LNM, lymph node metastasis; DM, distant metastasis; DOD, dead of disease; NED, no evidence of disease.

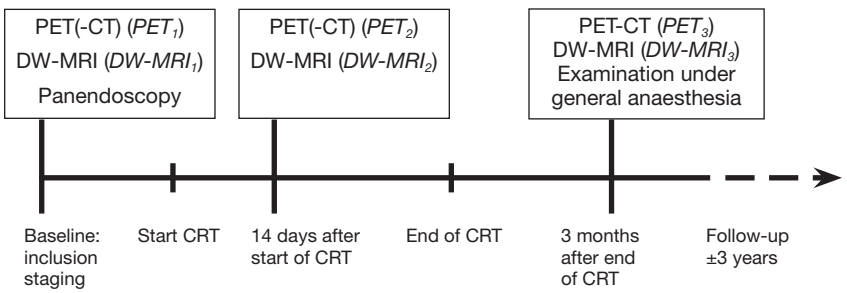

Figure 1 Timeline illustrating the consecutive methodological steps in the study.

methodological steps in the study is shown in *Figure 1*.

DW-MRI

MRI was performed using a 1.5 Tesla MR imaging system (Sonata; Siemens, Erlangen, Germany) with a head coil combined with a phased array spine and neck coil. After an axial short TI inversion-recovery (STIR)-series with 7-mm sections covering the entire neck area, subsequent images were centered on the area of interest containing the primary tumor and enlarged lymph nodes. Axial images (22 slices of 4-mm slice thickness and 0.4-mm gap, in-plane pixel size of 0.9 mm × 0.9 mm) were obtained with STIR (TR/TE/T1 =5,500/26/150 ms, 2 averages) and T1-weighted (T1WI) spin-echo (TR/TE =390/140 ms, 2 averages, no fat saturation) before and after the injection of contrast material. Gadovist (0.1 mL/kg of gadobutrol), Magnevist (0.2 mL/kg gadopentetate dimeglumine; both Bayer Schering Pharma, Berlin-Wedding, Germany) or Dotarem (0.2 mL/kg of gadoteric acid; Guerbet, Aulnay-sous Bois, France), was intravenously administered to obtain contrast-enhanced T1WI.

DWI with both EPI- and HASTE-techniques was obtained for the same 22 slices at the same slice position as the axial STIR and T1WI. Parameters for EPI were the following: TR/TE =5,000/105 ms, in-plane pixel size =2 mm × 2 mm, and b values =0, 500 and 1,000 s/mm^2 (3 averages). Parameters for HASTE were: TR/TE =900/110 ms, in-plane pixel size=1.1 mm × 1.1 mm, and b values =0 s/mm^2 (3 averages) and 1,000 s/mm^2 (12 averages). ADC maps of both EPI- and HASTE-DWI were calculated on-line or off-line, respectively, by using the software of the scanner.

18F-FDG-PET(-CT)

All patients fasted for at least 6 hours. Mean serum glucose levels were 6.5 mmol/L, with a range from 4.3 to 11.2 mmol/L. 186-367 MBq of 18F-FDG, depending on the body mass index and PET system used, was intravenously injected. PET_1 consisted of at least a whole-body PET (mid-femur to cranial vault) in all patients plus head and neck imaging (jugulum to orbit) in four patients, whereas PET_2 and PET_3

only comprised PET images of the head and neck region. In two patients, PET imaging was performed using a full-ring BGO PET scanner (ECAT EXACT HR+, CTI/Siemens, Erlangen, Germany; 2D-mode; 5 min emission scans/bed position, 2-min transmission scans using Ge-68 rod sources). PET-scanning started at sixty minutes (±15) post injection (p.i). of 18F-FDG. The PET-images were reconstructed using ordered subset expectation maximisation (OSEM) with 2 iterations and 16 subsets, an image matrix size of 128×128, resulting in voxel sizes of 5 mm × 5 mm. A 5-mm FWHM Gaussian post-reconstruction filter was applied, resulting in a final image resolution of 7 mm FWHM. During reconstruction all corrections needed for quantification were applied, such as decay, attenuation, scatter, dead time and normalisation corrections. In the other patients, PET-imaging was performed using an integrated PET-CT system (Gemini TF, Philips Medical Systems, Best, the Netherlands; 3D-mode; 2 min emission scans/bed position). Low dose CT scanning was performed with 120 kV and 50 mAs prior to emission scanning and used for attenuation correction of the emission scan and for anatomical localisation of FDG-avid lesions. In three patients, PET imaging was performed 60 minutes (±15) p.i. and in three patients PET was performed 90 minutes (±15) p.i. PET-CT data were reconstructed using a time of flight row-action maximum likelihood algorithm, as implemented by the vendor. Final image matrix size equals 170×170 with a voxel size of 4 mm × 4 mm × 4 mm. Final image resolution equalled 7 mm FWHM. Serial PET-CT studies in a single patient were performed using the same scanner, uptake time, acquisition and reconstruction protocols.

Analysis of MRI data

DW-MRI scans were analysed by a radiologist (J.A.C.) with 29 years of experience in head and neck radiology. Clinical information was provided about TNM stage, but the interpreter was blinded to clinical outcome. DW-MRI_1, DW-MRI_2 and DW-MRI_3 were simultaneous analysed on PACS (Sectra RIS/PACS version 12, Sectra Imtec AB, Linköping, Sweden) that allowed viewing of multiple MRI scans. All primary tumor and metastatic lymph nodes with a minimal axial diameter >5 mm were included. A lymph node was considered metastatic if proven by fine needle aspiration cytology or indicated by increased 18F-FDG uptake on PET(-CT) scan. All included lesions were identified on baseline images and corresponding lesions on DW-MRI_2 and DW-MRI_3 were identified by visual and slice position-based correlation. For each lesion, contours were manually drawn on the conventional MR images by J.A.C. around the lesional border at each slice position to measure total tumor volume. The volume of the lesions was calculated as the sum of the surfaces at each slice position multiplied by slice thickness and the interslice gap. Volume changes (ΔV_X) in % in relation to DW-MRI_1 were calculated using the formula:

$$\Delta V_X = [(V_X - V_B)/ V_B]*100$$

where V_B represents baseline volume and V_X represents volume on the X^{th} time point during or after treatment. A composite of all included lymph nodes was used to calculate the change in nodal volume.

Thereafter, ADC-values were calculated by drawing a region of interest (ROI) on a single slice of an axial EPI- and HASTE-ADC map, containing the largest available tumor area. The sets of DWI were evaluated independently from each other. For solid lesions, ROIs were drawn encompassing the entire lesion. In case of necrotic components, ROIs were drawn in that area of the lesion that showed contrast-enhancement in the corresponding post-contrast T1WI. ADC was measured before, during and after treatment in those patients with a residual enlarged lymph node. It was impossible to reliably draw a ROI if lymph node metastases had strongly shrunk due to the treatment. The lowest ADC-value of all pathologic lymph nodes in one patient (ADC_{low}) was considered a representative measure for follow-up, as suggested by Wahl *et al*. for PET (19). ADC-changes (ΔADC_X) in % in relation to baseline were calculated, similar to changes in volume.

Analysis of PET(-CT) data

PET images were independently interpreted by two nuclear medicine physicians with each 15 years PET experience (O.S.H. and E.F.C.) in head and neck oncology. PET-images were assessed on the presence of foci of increased activity within the tumor greater than surrounding background. PET readers had access to clinical information and DW-MRI_1 for anatomic correlation, but were blinded to the report of the radiologist and clinical outcome. PET(-CT) images were displayed on a standard workstation allowing simultaneous viewing of coronal, sagittal and transverse planes, with cross-referencing, as well as a 3-dimensional rotation projection. In case of discrepant interpretations a consensus was reached after discussion.

Standardized uptake values (SUV) were calculated as SUV_{max} (highest tumor voxel value within the lesion) and SUV_{mean} (average SUV within the lesion) by C.S.S., under

Table 2 ADC_{EPI}, ADC_{HASTE}, ΔSUV_{mean} and ΔSUV_{max} for primary tumors at baseline and early during treatment

No. of patient	Primary tumor					
	ADC_{EPI} MRI_1 ($\times 10^{-5}$ mm^2/s)	ADC_{EPI} MRI_2 ($\times 10^{-5}$ mm^2/s)	ADC_{HASTE} MRI_1 ($\times 10^{-5}$ mm^2/s)	ADC_{HASTE} MRI_2 ($\times 10^{-5}$ mm^2/s)	ΔSUV_{mean} PET_{1-2} (%)	ΔSUV_{max} PET_{1-2} (%)
1	84	117	114	111	15.9	15.8
2	85	102	106	128	NA[1]	NA[1]
3	104	134	70	73	NA[2]	NA[2]
4	77	143	58	73	–74.5	–79.5
5	NA[3]	NA[3]	NA[3]	NA[3]	NA[3]	NA[3]
6	56	57	85	74	–69.1	–69.4
7	77	98	74	54	–54.4	–54.9
8	66	113	65	78	NA[4]	NA[4]

[1], PET_1 was performed without a transmission scan; [2], PET_1 was reconstructed with an aberrant voxel size; [3], no primary tumor; [4], PET_2 was not performed; NA, not applicable.

supervision of O.S.H., measured in the primary tumors and in the (up to 3) largest lymph nodes, using previously described methodology (20). SUVs were normalized for body weight and serum glucose. If, after treatment, no lesions with increased 18F-FDG uptake were visible, a ROI of 3×3×3 voxels was drawn at the initial location of the primary tumor and/or lymph nodes. SUV-changes (ΔSUV_X) in % in relation to baseline were calculated.

Statistics

Statistical analyses were performed using SPSS software package (version 20.0; IBM Corp., Armonk, NY, USA). The level of significance was set at $P<0.05$. A two-sided nonparametric exact Wilcoxon signed rank test was used for paired data comparisons between primary tumor parameters from the first and second DW-MRI or 18F-FDG-PET(-CT). A two-sided Mann-Whitney U test was used for group comparisons; regional control versus regional recurrent disease. To evaluate correlations between ΔADC and ΔSUV, a Spearman's correlation coefficient was used.

Results

Imaging

DW-imaging before and during treatment was conducted in all patients according to the study protocol. PET(-CT) imaging and reconstruction was not correctly performed in all patients due to different logistic difficulties, as indicated in *Tables 2,3*. All primary tumors were detected with DW-MRI (both EPI- and HASTE-technique) and PET(-CT) except in one patient, in whom the primary tumor had been resected transorally in another hospital. ADC- and ΔSUV-values of the primary tumor and nodal metastases at baseline and during treatment are shown in *Tables 2,3*.

Treatment outcome

Six out of eight patients remained disease-free during follow-up. In two patients a regional recurrence was diagnosed; at 17 and 29 months posttreatment. No local recurrences were detected. One salvage neck dissection was performed with histopathologically proven lymph node metastases in the surgical specimen. In the other patient, regional recurrence was presumed on the basis of clinical examination and ultrasound imaging. This patient died (of a carotid blow-out) before histopathological diagnosis was obtained.

Primary tumor

Figure 2 represents the pattern of change in ADC_{EPI} and ADC_{HASTE}. With EPI-DWI, six patients showed a substantial ADC-increase from $DW\text{-}MRI_1$ to $DW\text{-}MRI_2$, whereas ADC_{EPI} increased with only 1.8% in patient 6 on $DW\text{-}MRI_2$. With HASTE-DWI, three patients showed a substantial ADC-increase on $DW\text{-}MRI_2$ compared to $DW\text{-}MRI_1$. ADC-values in the other four patients did not show a substantial increase or showed a decrease. Volume, ADC-, ΔADC- and ΔSUV-values of the primary tumors are listed in *Table 4*. Median pretreatment ADC_{EPI} was 77×10^{-5} (SD 15.2) mm^2/s,

Table 3 ADC_{EPI}, ADC_{HASTE}, ΔSUV_{mean} and ΔSUV_{max} for nodal metastases at baseline and early during treatment

No. of patient	Lymph node metastases*‡					
	ADC_{EPI} MRI_1 ($\times 10^{-5}$ mm^2/s)	ADC_{EPI} MRI_2 ($\times 10^{-5}$ mm^2/s)	ADC_{HASTE} MRI_1 ($\times 10^{-5}$ mm^2/s)	ADC_{HASTE} MRI_2 ($\times 10^{-5}$ mm^2/s)	ΔSUV_{mean} PET_{1-2} (%)	ΔSUV_{max} PET_{1-2} (%)
1	93	101	101	107	39.1	28.7
2	80	121	103	136	NA[1]	NA[1]
3	109	124	84	68	NA[2]	NA[2]
4	67	93	41	74	–51.1	–62.2
5	89	121	66	89	–39.4	–42.7
6	78	95	67	71	–25.7	–30.4
7	72	125	71	93	–37.9	–38.2
8	108	120	91	110	NA[3]	NA[3]

*, the lowest ADC-value of all included lymph nodes in one patient; ‡, the highest SUV-value of all included lymph nodes in one patient; [1], PET_1 was performed without a transmission scan; [2], PET_1 was reconstructed with an aberrant voxel size; [3], PET_2 was not performed; NA, not applicable.

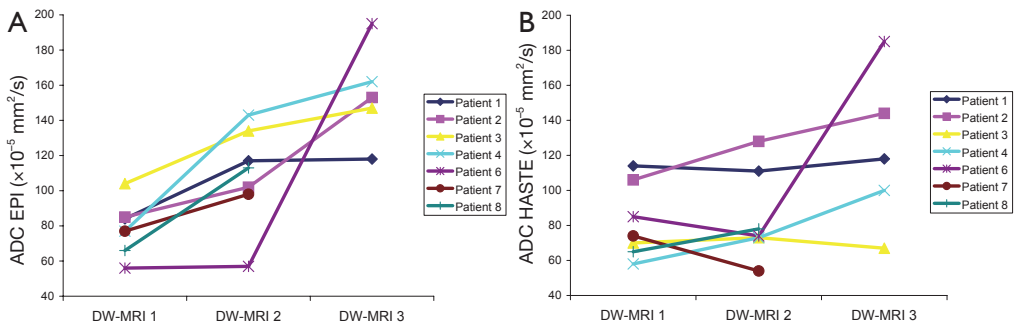

Figure 2 Patterns of change in ADC_{EPI} (A) and ADC_{HASTE} (B) between $DW\text{-}MRI_1$, $DW\text{-}MRI_2$ and $DW\text{-}MRI_3$ of the primary tumor. The DW-MRI after treatment was not conducted using study protocol in patient 7 and patient 8.

Table 4 Volume, ADC-values, ΔADC and ΔSUV of the primary tumor. Values are expressed as median [range]

	Volume* (cm^3)	ADC_{EPI} ($\times 10^{-5}$ mm^2/s)	ADC_{HASTE} ($\times 10^{-5}$ mm^2/s)	ΔADC_{EPI} (%)	ΔADC_{HASTE} (%)	ΔSUV_{max} (%)	ΔSUV_{mean} (%)
$DW\text{-}MRI_1$ (n=7)	117.0 [45.2; 240.0]	77 [56; 104]	74 [58; 114]				
$DW\text{-}MRI_2$ (n=7)	16.1 [8.7; 148.8][a]	113 [57; 143][a]	74 [54; 128]				
$DW\text{-}MRI_3$ (n=5)	4.0 [0; 33.9][a,b]	153 [118; 195]	118 [67; 185]				
$DW\text{-}MRI_{1-2}$ (n=7)				28.8 (1.8; 85.7)	4.3 (–27.0; 25.9)		
$DW\text{-}MRI_{1-3}$ (n=5)				80.0 (40.5; 248.2)	35.8 (–4.3; 117.7)		
PET_{1-2} (n=4)						–62.1 (–79.5; 15.8)	–61.7 (–75.4; 15.9)
PET_{1-3} (n=5)						–80.4 (–88.3; –72.9)	–80.0 (–86.2; –69.5)

*, based on MRI; [a], P<0.05 compared with DW-MRI1; [b], n=7.

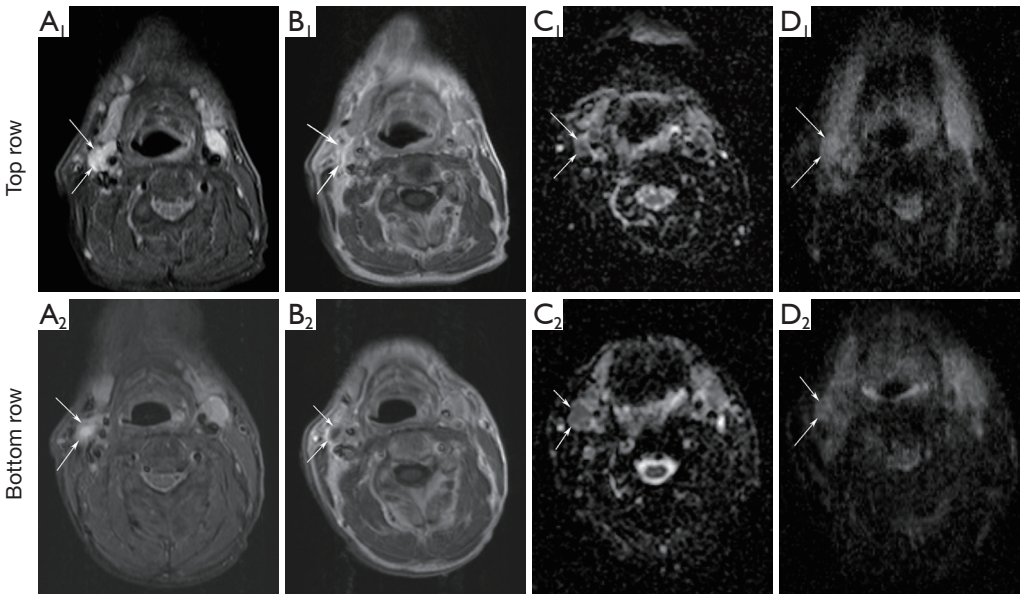

Figure 3 Axial images showing a metastatic node (arrows) in patient number 1 in whom recurrent viable squamous cell carcinoma was diagnosed histopathologically in level II right during follow-up. DW-MRI$_1$ (top row) and DW-MRI$_2$ (bottom row): (A) STIR; (B) contrast-enhanced T1WI; (C) ADC maps with EPI technique and (D) ADC maps with HASTE technique. ADC$_{EPI}$-values of the lymph node (arrow) are 99×10^{-5} and 102×10^{-5} mm^2/s for DW-MRI$_1$ and DW-MRI$_2$, respectively. ADC$_{HASTE}$-values are 106×10^{-5} and 118×10^{-5} mm^2/s. Four years after completion of CRT this patient died due to lung metastases.

significantly increasing to 113×10^{-5} (SD 27.8) mm^2/s (P=0.02) early during treatment. Median ADC$_{HASTE}$ values were 74×10^{-5} (SD 21.1) mm^2/s and 74×10^{-5} (SD 25.6) mm^2/s.

Visual interpretation of PET$_2$ still showed a focus of increased activity within the tumor in four patients. ΔSUV_{max} decreased with 62.1%±43.1% (median ± SD) and ΔSUV_{mean} with 61.7±41.8 from PET$_1$ to PET$_2$.

Lymph node metastases

An example of DW-MRI$_1$ and DW-MRI$_2$ in a patient with a regional recurrence is shown in *Figure 3*. At baseline, median ADC-values of patients with regional control (ADC$_{EPI}$: 87.5×10^{-5} mm^2/s and ADC$_{HASTE}$: 76.7×10^{-5} mm^2/s) and those with recurrent disease (ADC$_{EPI}$: 85.5×10^{-5} mm^2/s and ADC$_{HASTE}$: 84.0×10^{-5} mm^2/s) were similar (P=0.89 and P=0.74, respectively). At DW-MRI$_2$, ADC$_{low}$ with EPI tended to be (not statistically significant, P=0.18) higher for six patients with regional control [(117.3±12.1)×10^{-5} mm^2/s] than for the patients with a recurrence [(98.0±4.2)×10^{-5} mm^2/s]. With HASTE-DWI this difference was not seen [(93.5±26.7)×10^{-5} versus (89.0±25.5)×10^{-5} mm^2/s, P=0.74] (*Figure 4A*). $\Delta ADC_{low\text{-}2weeks}$ with EPI tended to be higher for patients with regional control than for recurrences (37.4%±23.5% versus 15.2%±9.3%, P=0.18). $\Delta ADC_{low\text{-}2weeks}$ with HASTE also tended to be higher for patients with regional control (27.4%±27.1% versus 6.0%±0.02%, P=0.18) (*Figure 4B*).

$\Delta Volume_{2weeks}$ in six patients with regional control was –38.9%±42.5% (mean±SD) and 13.0%±9.2% in the two patients with a lymph node recurrence (P=0.74). Both patients with a regional recurrence were visually interpreted as a non-complete response on PET$_2$. Of the patients with regional control, in two patients no focus of increased activity within the lymph nodes was seen, whereas in three patients a focus was still seen. A trend was seen for more change in SUV_{max} in patients with regional control than in patients with a regional recurrence. $\Delta SUV_{max\text{-}2weeks}$ in regional control was –47.7%±12.7% and –0.8%±41.8% in regional recurrences. $\Delta SUV_{mean\text{-}2weeks}$ in patients with regional control was –42.8%±7.2% and 6.7%±45.8% in patients with a recurrence (P=0.08) (*Figure 4C*).

Correlation between ADC and SUV

For the primary tumors, no correlation were found

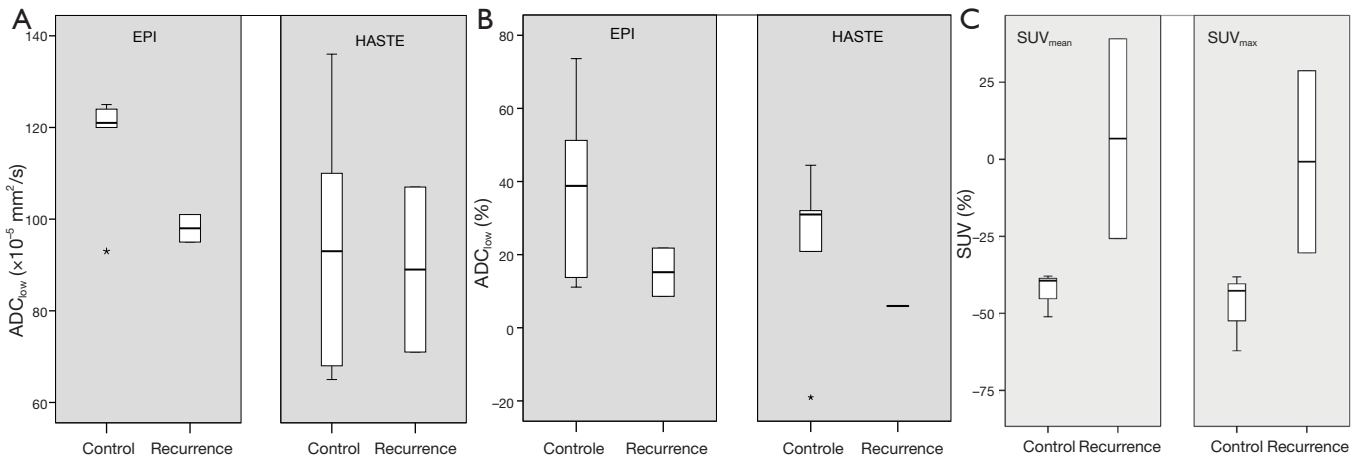

Figure 4 Comparison of lymph node (A) ADC_{low} at $DW\text{-}MRI_2$, (B) $\Delta ADC_{low\text{-}2weeks}$ (in %) and (C) ΔSUV_{2weeks} (in %), in six patients with regional control and two patients with recurrent disease. Box-whisker plots are presented with median (–), interquartile range (box), and range (–).

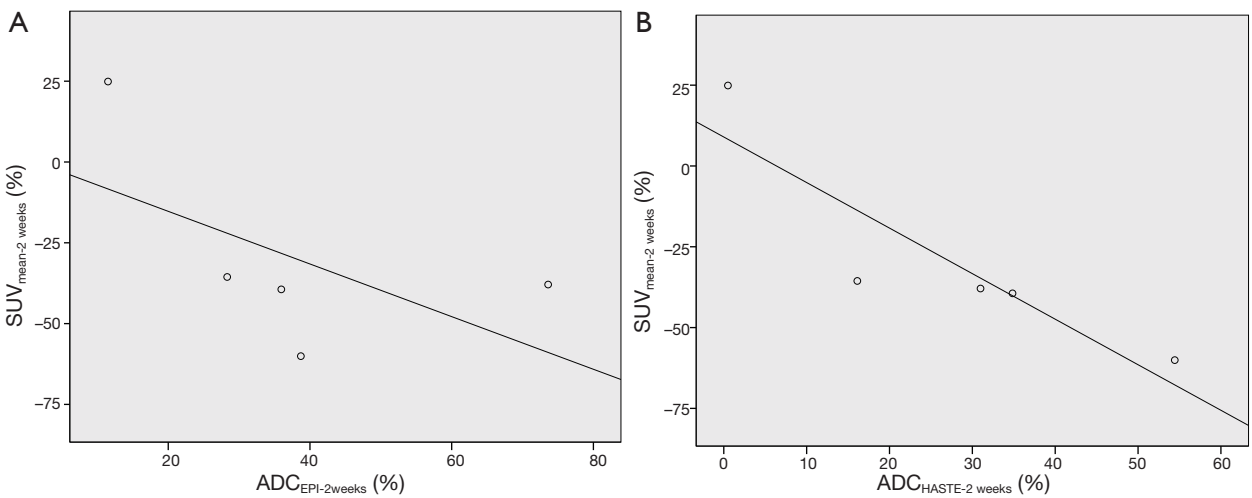

Figure 5 Correlation for the lymph node metastases between (A) $\Delta ADC_{EPI\text{-}2weeks}$ and $\Delta SUV_{mean\text{-}2weeks}$ and (B) $\Delta ADC_{HASTE\text{-}2weeks}$ and $\Delta SUV_{mean\text{-}2weeks}$.

between $\Delta ADC_{EPI\text{-}2weeks}$ and $\Delta SUV_{mean\text{-}2weeks}$ or $\Delta SUV_{max\text{-}2weeks}$ (P=0.80) or between $\Delta ADC_{HASTE\text{-}2weeks}$ and $\Delta SUV_{mean\text{-}2weeks}$ or $\Delta SUV_{max\text{-}2weeks}$ (P=0.60). For the lymph node metastases, no correlation was seen in $\Delta ADC_{EPI\text{-}2weeks}$ and $\Delta SUV_{mean\text{-}2weeks}$ (spearman's rho =–0.70, P=0.19) or $\Delta SUV_{max\text{-}2weeks}$ (spearman's rho =–0.40, P=0.6). A significant negative correlation was found between $\Delta ADC_{HASTE\text{-}2weeks}$ and $\Delta SUV_{max\text{-}2weeks}$ (spearman's rho =–0.90, P=0.04) and $\Delta SUV_{mean\text{-}2weeks}$ (spearman's rho =–1.0, P=0.01) (*Figure 5*).

Discussion

CRT is a standard therapeutic option for patients with advanced stage HNSCC, also if technically resectable. Identification of non-responders early during CRT may spare a number of patients from a futile extensive treatment. Several results in HNSCC studies suggest that changes in ADC measured with an EPI-DWI technique early during CRT are associated with locoregional response (11-13). However, EPI-DWI suffers from geometrical distortions, especially in regions with air-tissue transitions such as in the head and neck area. Consequently, the use of EPI-DWI in radiotherapy planning and in simultaneous PET/MRI imaging may be limited. In this pilot study, we wanted to explore the use of a non-EPI DWI method, because such DWI sequences are more robust concerning geometric

accuracy. We compared EPI-DWI with HASTE-DWI early during CRT for their potential to predict locoregional outcome. Our preliminary results suggest that EPI-DWI seems to have greater potential in predicting locoregional outcome early after start of CRT than HASTE-DWI. Although HASTE-DWI has a lower incidence of geometric distortions as compared to an EPI-DWI (15), this technique seems to fail in early CRT response prediction in HNSCC.

CRT induces loss of tumor cells and thus increases water mobility at the microscopic level. Response to treatment corresponds to an increase in ADC. This treatment-induced ADC-increase has been confirmed in several HNSCC-studies. Kim *et al*. showed a significant ADC increase in responding, compared to non-complete responding metastatic lymph nodes from HNSCC, one week after initiation of radiotherapy (11). Unlike the study of Kim *et al*., our DWI sequences covered the neck completely instead of only the metastatic lymph node and analysis also included the primary tumor. In a second study, King *et al*. analysed primary tumors and lymph nodes together, without differentiating these entities and showed that serial changes in tumor ADC, obtained over the course of treatment, provided a marker for treatment response. A fall in ADC during treatment correlated with locoregional failure (13). In another study with 30 patients, Vandecaveye *et al*. concluded that ADC-changes of the primary tumor and lymph nodes at 2 and 4 weeks after the start of CRT were significantly associated with locoregional response, in contrast to the change in volume (12). In the head and neck region, DWI is generally performed with an EPI-sequence, as in previous described studies. Our findings using EPI-DWI are compatible with these HNSCC-studies. In contrary to previous studies, we evaluated DWI as a technique to predict treatment response with both EPI- and HASTE-DWI, to explore the application of a non-EPI sequence in this area of research.

DWI is particularly difficult in this region, because it contains a variety of tissues, including bone, fat, muscle, glandular tissue and air. Moreover, movement-related problems, like swallowing, breathing, coughing, speaking and jaw movements impede imaging of the head and neck. This can produce images with strong susceptibility artefacts. EPI-DWI is sensitive to geometric distortions, which is especially strong near interfaces between soft tissue and air or bone. Functional imaging has a crucial role in accurate tumor delineation and defining the targets for radiotherapy planning. 18F-FDG-PET-CT is commonly used for treatment planning. DW-MRI might has additional value in treatment planning, because DW-MRI can distinguish between reactively enlarged lymph nodes and metastatic lymph nodes (21). Therefore, DW images without geometric distortions are important for fusing PET images with DWI. If artefacts are too detrimental, a non-EPI technique can be used instead of an EPI-technique. MR images performed with an EPI- or non-EPI method, vary concerning contrast, signal-to-noise ratio (SNR) and artefarcts. In HNSCC, Verhappen *et al*. showed that primary tumors and metastatic lymph nodes are more easily visualized on EPI-DWI compared to HASTE-DWI due to a higher SNR. However, EPI-DWI demonstrated more frequent susceptibility artefacts resulting in geometric distortions (14,15). In the present study, we performed both EPI- and HASTE-DWI. As stated above, EPI-DWI might have greater potential in predicting locoregional outcome and HASTE-DWI seems to provide inadequate information. Up to now, it is uncertain which DWI-technique is most appropriate in head-and-neck imaging. However, our study contributes to the general opinion that EPI-DWI probably is the most promising technique in oncologic imaging in the head and neck region. Therefore, further optimization of the EPI-DWI sequence is necessary to reduce image distortions and in order to make this technique useful in radiotherapy planning and simultaneous PET/MRI imaging.

18F-FDG-PET-CT is another possible modality for treatment prediction. Controversial results on the accuracy of PET to predict treatment outcome in HNSCC patients have been reported. Several authors have concluded that changes in FDG-uptake levels during non-surgical treatment are associated with tumor response, locoregional control and overall survival (16-18). However, Castaldi *et al*. could not confirm a predictive role for PET-CT performed after 2 weeks of CRT (22). Ceulemans *et al*. found a low sensitivity for FDG-PET after 47 Gy (23). The interpretation of PET-images can be difficult because of false positive findings, as tracer uptake can also occur in normal tissues, inflammatory tissue or reactive lymph nodes. Besides, optimal timing to assess response with PET-CT during radiotherapy remains a matter of debate, since increases in 18F-FDG-uptake early during treatment have been reported due to radiation-induced inflammatory responses and repair processes (24). We performed PET(-CT) after 20 Gy. At this time, radiotherapy-induced inflammation and 18F-FDG accumulation in the activated macrophages is assumed to be low (25). Most aforementioned studies are performed with stand-alone

PET, while PET-CT is the current 'state of the art'. In the present study PET-CT was performed in most patients, using CT to improve the optimal delineation of the primary tumor and lymph node metastases (ROI).

DW-MRI and 18F-FDG-PET-CT are both imaging techniques used in oncology and have similar clinical applications. However, both modalities represent different aspects of tumor biology; ADC representing tissue cellularity and SUV representing glucose metabolism. A few studies in HNSCC assessed the correlation between pretreatment ADC-values and SUV-values. Nakajo *et al.* demonstrated a significant inverse correlation between primary tumor SUV_{max} and ADC in 26 patients (26). Nakamatsu *et al.* demonstrated this negative correlation between SUV_{max} and ADCmin also in 41 metastatic lymph nodes (27). Opposite, Fruehwald-Pallamar *et al.* and Varoquaux *et al.* did not find a correlation between primary tumor ADC and SUV (28,29). Our present pilot study is the first study to compare changes in ADC and SUV between pretreatment and early during treatment. For the primary tumor, no correlations between ΔADC (with EPI- and HASTE-DWI) and ΔSUV were found. The results for the nodal metastases demonstrated no correlation between ΔADC_{EPI} and ΔSUV. A significant negative correlation was found between ΔADC_{HASTE} and ΔSUV. Our results suggest that both EPI-DWI and 18F-FDG-PET-CT might provide independent information in the early response to treatment, since no correlations were found. Both techniques could play a different role in clinical assessment, in contrast to HASTE-DWI which seems to provide the same information as 18F-FDG-PET(-CT), since significant correlations were found between ΔADC_{HASTE} and ΔSUV. Therefore, a combination of EPI-DWI and PET might be promising in predictive and follow-up studies of HNSCC and with simultaneous PET/MRI imaging spreading in the clinical field, both techniques can be combined in one single scanner.

We acknowledge several limitations to this study. First, this pilot study had an exploratory character and was conducted with a small number of patients. Although a limited number of patients was included, this is the first study to evaluate the potential predictive value of two DWI-techniques and 18F-FDG-PET(-CT) with follow-up. Multiple tumors (primary and metastases) in a single patient were analysed independently to offset this small number of patients, resulting in 32 tumors. Second, in our patient cohort no local recurrences occurred during follow-up. Therefore, it is difficult to investigate the role of DW-MRI and 18F-FDG-PET(-CT) as an imaging tool to predict local outcome. However, in our preliminary results ADC_{EPI} from the primary tumors showed the expected significant increase from baseline to early during treatment, in contrast to ADC_{HASTE}. Third, we evaluated the DWI-images by whole-tumor mean ADC-value. The accuracy of DW-MRI can possibly be improved by expanding these calculations with data on skewness and kurtosis, taking tumor heterogeneity into account (30) or a voxel-wise approach with parametric response maps (31). Finally, we were not able to report absolute SUV-values since we applied two different uptake intervals (60 and 90 minutes); changes of SUV are more robust provided that the same conditions prevailed during serial imaging per patient, and this was the case in our study.

Our preliminary results suggest that HASTE-DWI seems to be inadequate in early response prediction, compared to EPI-DWI which has greater potential to predict locoregional outcome after CRT. EPI-DWI and 18F-FDG-PET-CT could potentially provide independent information in the early response to treatment, since no correlations were found between ΔADC_{EPI} and ΔSUV. This is in contrast to ADC-HASTE, which appears to provide similar information as 18F-FDG-PET-CT, because significant correlations were found between ΔADC_{HASTE} and ΔSUV.

Acknowledgements

We would like to thank Prof. Dr. R. Boellaard for his assistance in reconstructing PET-data.

Author contribution: CSS: [1] data acquisition, data analysis, [2] drafting the article, [3] final approval; RdB: [1] conception and design, [2] revising the article critically, [3] final approval; LvdP: [1] data acquisition, [2] revising the article critically, [3] final approval; DPN: [1] data interpretation, [2] revising the article critically, [3] final approval; OSH: [1] data interpretation, [2] revising the article critically, [3] final approval; EFC: [1] data interpretation, [2] revising the article critically, [3] final approval; BIW: [1] data analysis, [2] revising the article critically, [3] final approval; PAD: [1] conception and design, [2] revising the article critically, [3] final approval; CRL: [1] conception and design, [2] revising the article critically, [3] final approval; JAC: [1] conception and design, data interpretation, [2] revising the article critically, [3] final approval.

Disclosure: The authors declare no conflict of interest.

References

1. Argiris A, Karamouzis MV, Raben D, Ferris RL. Head and neck cancer. Lancet 2008;371:1695-709.
2. Bonner JA, Harari PM, Giralt J, Azarnia N, Shin DM, Cohen RB, Jones CU, Sur R, Raben D, Jassem J, Ove R, Kies MS, Baselga J, Youssoufian H, Amellal N, Rowinsky EK, Ang KK. Radiotherapy plus cetuximab for squamous-cell carcinoma of the head and neck. N Engl J Med 2006;354:567-78.
3. Pignon JP, Bourhis J, Domenge C, Designé L. Chemotherapy added to locoregional treatment for head and neck squamous-cell carcinoma: three meta-analyses of updated individual data. MACH-NC Collaborative Group. Meta-Analysis of Chemotherapy on Head and Neck Cancer. Lancet 2000;355:949-55.
4. Lavertu P, Bonafede JP, Adelstein DJ, Saxton JP, Strome M, Wanamaker JR, Eliachar I, Wood BG. Comparison of surgical complications after organ-preservation therapy in patients with stage III or IV squamous cell head and neck cancer. Arch Otolaryngol Head Neck Surg 1998;124:401-6.
5. Newman JP, Terris DJ, Pinto HA, Fee WE Jr, Goode RL, Goffinet DR. Surgical morbidity of neck dissection after chemoradiotherapy in advanced head and neck cancer. Ann Otol Rhinol Laryngol 1997;106:117-22.
6. De Bree R. Functional imaging to predict treatment response after (chemo) radiotherapy of head and neck squamous cell carcinoma. Quant Imaging Med Surg 2013;3:231-4.
7. Koh DM, Collins DJ. Diffusion-weighted MRI in the body: applications and challenges in oncology. AJR Am J Roentgenol 2007;188:1622-35.
8. Bammer R. Basic principles of diffusion-weighted imaging. Eur J Radiol 2003 ;45:169-84.
9. Ross BD, Moffat BA, Lawrence TS, Mukherji SK, Gebarski SS, Quint DJ, Johnson TD, Junck L, Robertson PL, Muraszko KM, Dong Q, Meyer CR, Bland PH, McConville P, Geng H, Rehemtulla A, Chenevert TL. Evaluation of cancer therapy using diffusion magnetic resonance imaging. Mol Cancer Ther 2003;2:581-7.
10. Hamstra DA, Lee KC, Moffat BA, Chenevert TL, Rehemtulla A, Ross BD. Diffusion magnetic resonance imaging: an imaging treatment response biomarker to chemoradiotherapy in a mouse model of squamous cell cancer of the head and neck. Transl Oncol 2008;1:187-94.
11. Kim S, Loevner L, Quon H, Sherman E, Weinstein G, Kilger A, Poptani H. Diffusion-weighted magnetic resonance imaging for predicting and detecting early response to chemoradiation therapy of squamous cell carcinomas of the head and neck. Clin Cancer Res 2009;15:986-94.
12. Vandecaveye V, Dirix P, De Keyzer F, de Beeck KO, Vander Poorten V, Roebben I, Nuyts S, Hermans R. Predictive value of diffusion-weighted magnetic resonance imaging during chemoradiotherapy for head and neck squamous cell carcinoma. Eur Radiol 2010;20:1703-14.
13. King AD, Mo FK, Yu KH, Yeung DK, Zhou H, Bhatia KS, Tse GM, Vlantis AC, Wong JK, Ahuja AT. Squamous cell carcinoma of the head and neck: diffusion-weighted MR imaging for prediction and monitoring of treatment response. Eur Radiol 2010;20:2213-20.
14. Schakel T, Hoogduin JM, Terhaard CH, Philippens ME. Diffusion weighted MRI in head-and-neck cancer: geometrical accuracy. Radiother Oncol 2013;109:394-7.
15. Verhappen MH, Pouwels PJ, Ljumanovic R, Van der Putten L, Knol DL, De Bree R, Castelijns JA. Diffusion-weighted MR imaging in head and neck cancer: comparison between half-fourier acquired single-shot turbo spin-echo and EPI techniques. AJNR Am J Neuroradiol 2012;33:1239-46.
16. Brun E, Kjellén E, Tennvall J, Ohlsson T, Sandell A, Perfekt R, Perfekt R, Wennerberg J, Strand SE. FDG PET studies during treatment: prediction of therapy outcome in head and neck squamous cell carcinoma. Head Neck 2002;24:127-35.
17. Farrag A, Ceulemans G, Voordeckers M, Everaert H, Storme G. Can 18F-FDG-PET response during radiotherapy be used as a predictive factor for the outcome of head and neck cancer patients? Nucl Med Commun 2010;31:495-501.
18. Hentschel M, Appold S, Schreiber A, Abolmaali N, Abramyuk A, Dörr W, Kotzerke J, Baumann M, Zöphel K. Early FDG PET at 10 or 20 Gy under chemoradiotherapy is prognostic for locoregional control and overall survival in patients with head and neck cancer. Eur J Nucl Med Mol Imaging 2011;38:1203-11.
19. Wahl RL, Jacene H, Kasamon Y, Lodge MA. From RECIST to PERCIST: Evolving Considerations for PET response criteria in solid tumors. J Nucl Med 2009;50 Suppl 1:122S-50S.
20. Krak NC, Boellaard R, Hoekstra OS, Twisk JW, Hoekstra CJ, Lammertsma AA. Effects of ROI definition and reconstruction method on quantitative outcome and

applicability in a response monitoring trial. Eur J Nucl Med Mol Imaging 2005;32:294-301.
21. Vandecaveye V, De Keyzer F, Vander Poorten V, Dirix P, Verbeken E, Nuyts S, Hermans R. Head and neck squamous cell carcinoma: value of diffusion-weighted MR imaging for nodal staging. Radiology 2009;251:134-46.
22. Castaldi P, Rufini V, Bussu F, Miccichè F, Dinapoli N, Autorino R, Lago M, De Corso E, Almadori G, Galli J, Paludetti G, Giordano A, Valentini V. Can "early" and "late"18F-FDG PET-CT be used as prognostic factors for the clinical outcome of patients with locally advanced head and neck cancer treated with radio-chemotherapy? Radiother Oncol 2012;103:63-8.
23. Ceulemans G, Voordeckers M, Farrag A, Verdries D, Storme G, Everaert H. Can 18-FDG-PET during radiotherapy replace post-therapy scanning for detection/demonstration of tumor response in head-and-neck cancer? Int J Radiat Oncol Biol Phys 2011;81:938-42.
24. Bussink J, van Herpen CM, Kaanders JH, Oyen WJ. PET-CT for response assessment and treatment adaptation in head and neck cancer. Lancet Oncol 2010;11:661-9.
25. Hentschel M, Appold S, Schreiber A, Abramyuk A, Abolmaali N, Kotzerke J, Baumann M, Zöphel K. Serial FDG-PET on patients with head and neck cancer: implications for radiation therapy. Int J Radiat Biol 2009;85:796-804.
26. Nakajo M, Nakajo M, Kajiya Y, Tani A, Kamiyama T, Yonekura R, Fukukura Y, Matsuzaki T, Nishimoto K, Nomoto M, Koriyama C. FDG PET/CT and diffusion-weighted imaging of head and neck squamous cell carcinoma: comparison ofprognostic significance between primary tumor standardized uptake value and apparent diffusioncoefficient. Clin Nucl Med 2012;37:475-80.
27. Nakamatsu S, Matsusue E, Miyoshi H, Kakite S, Kaminou T, Ogawa T. Correlation of apparent diffusion coefficients measured by diffusion-weighted MR imaging and standardized uptake values from FDG PET/CT in metastatic neck lymph nodes of head and neck squamous cell carcinomas. Clin Imaging 2012;36:90-7.
28. Fruehwald-Pallamar J, Czerny C, Mayerhoefer ME, Halpern BS, Eder-Czembirek C, Brunner M, Schuetz M, Weber M, Fruehwald L, Herneth AM. Functional imaging in head and neck squamous cell carcinoma: correlation of PET/CT and diffusion-weighted imaging at 3 Tesla. Eur J Nucl Med Mol Imaging 2011;38:1009-19.
29. Varoquaux A, Rager O, Lovblad KO, Masterson K, Dulguerov P, Ratib O, Becker CD, Becker M. Functional imaging of head and neck squamous cell carcinoma with diffusion-weighted MRI and FDG PET/CT: quantitative analysis of ADC and SUV. Eur J Nucl Med Mol Imaging 2013;40:842-52.
30. King AD, Chow KK, Yu KH, Mo FK, Yeung DK, Yuan J, Bhatia KS, Vlantis AC, Ahuja AT. Head and neck squamous cell carcinoma: diagnostic performance of diffusion-weighted MR imaging for the prediction of treatment response. Radiology 2013;266:531-8.
31. Galbán CJ, Mukherji SK, Chenevert TL, Meyer CR, Hamstra DA, Bland PH, Johnson TD, Moffat BA, Rehemtulla A, Eisbruch A, Ross BD. A feasibility study of parametric response map analysis of diffusion-weighted magnetic resonance imagingscans of head and neck cancer patients for providing early detection of therapeutic efficacy. Transl Oncol 2009;2:184-90.

Cite this article as: Schouten CS, de Bree R, van der Putten L, Noij DP, Hoekstra OS, Comans EF, Witte BI, Doornaert PA, Leemans CR, Castelijns JA. Diffusion-weighted EPI- and HASTE-MRI and 18F-FDG-PET-CT early during chemoradiotherapy in advanced head and neck cancer. Quant Imaging Med Surg 2014;4(4):239-250. doi: 10.3978/j.issn.2223-4292.2014.07.15

